Performance and Stability in H$_2$S of SrFe$_{0.75}$Mo$_{0.25}$O$_{3-\delta}$ as Electrode in Proton Ceramic Fuel Cells

S. Wachowski[1,2]*, Z. Li[3], J.M. Polfus[3], T. Norby[2]

[1] *Faculty of Applied Physics and Mathematics, Department of Solid State Physics, Gdansk University of Technology, ul. Narutowicza 11/12, 80-233 Gdansk, Poland*

[2] *Department of Chemistry, Centre for Materials Science and Nanotechnology, University of Oslo, FERMiO, Gaustadalléen 21, NO-0349 Oslo, Norway*

[3] *SINTEF Materials and Chemistry, PO Box 124 Blindern, NO-0314 Oslo, Norway*

*corresponding author: swachowski@mif.pg.gda.pl,

Abstract

The H$_2$S-tolerance of SrFe$_{0.75}$Mo$_{0.25}$O$_{3-\delta}$ (SFM) electrodes has been investigated in symmetric proton ceramic fuel cells (PCFC) with BaZr$_{0.8}$Ce$_{0.1}$Y$_{0.1}$O$_{3-\delta}$ (BZCY81) electrolyte. The ionic conductivity of the electrolyte under wet reducing conditions was found to be insignificantly affected in the presence of up to 5000 ppm H$_2$S. The fuel cell exhibited an OCV of about 0.9 V at 700 °C, which dropped to about 0.6 V and 0.4 V upon exposure to 500 and 5000 ppm H$_2$S, respectively, on the fuel side. Post characterization of the fuel cell revealed significant degradation of the anode in terms of microstructure and chemical composition due to formation of sulfides such as SrS, MoS$_2$ and Fe$_3$S$_4$. Nevertheless, the fuel cell was still functional due to the sufficient electronic conductivity of some of these sulfides.

Keywords: proton ceramic fuel cells (PCFC), sulfur tolerance, H$_2$S, strontium ferrite, barium zirconate

1. Introduction

Fuel cells represent a clean and efficient technology of converting chemical to electrical energy in which H$_2$ fuel is electrochemically converted with air to H$_2$O, electricity and heat [1]. Apart from hydrogen, these electrochemical devices can utilize various hydrogen containing fuels [2,3], of which biogas is of particular interest [4]. The exact composition of the biogas is important for its further application and this highly depends on the production process and type of organic matter [5]. Biogas typically consists of 35 – 75 vol.% of methane and 25 – 40 vol.% of carbon dioxide with small amounts of other components such as water vapour and H$_2$S [5,6]. The H$_2$S concentration in biogas is typically in the range of tens to thousands ppm, and can

reach up to 2 vol.% in extreme cases [5–8]. The presence of H_2S in the biogas is considered to be especially troublesome due to its corrosive nature and threat to health and environment, and it can form even more toxic and environmentally hazardous compounds such as SO_2, SO_3, and H_2SO_4 [6,9,10]. In fuel cells, H_2S can poison or lead to decomposition of fuel side electrodes [11–14], and it is particularly detrimental to the performance of Ni, a common anode component [12–14]. While gas purification processes such as chemical absorption, scrubbing, or biological purification can be applied to remove H_2S, these processes can be limited by scalability, low sustainability or high investment and/or running costs [6–8,10,15,16]. Furthermore, single-step purification processes cannot easily offer sufficient gas purity for fuel cell technologies, which typically requires H_2S concentrations lower than 1 ppm [10,15]. The prospect of H_2S tolerant anode materials is therefore particularly attractive.

Biogas can be converted into hydrogen via dry or steam reforming. Both processes require temperatures in the range of 600 – 800 °C in order to achieve high conversion and prevent carbon deposition [17–22]. Fuel cells operating in this temperature range therefore open the possibility for direct reforming of biogas. Moreover, it has been shown that formation of sulfides is restrained at temperatures above 500 °C [14], which makes high temperature devices promising in terms of H_2S tolerance.

Solid electrolyte fuel cells operating at high temperatures comprise the solid oxide fuel cell (SOFC) and proton ceramic fuel cell (PCFC). The former utilizes an oxide ion conducting electrolyte in which oxide ions migrate from the cathode to the anode. At the anode, the oxide ions may react with H_2S to form SO_2 and H_2O. In PCFCs on the other hand, protons migrate from the anode to the cathode, where they react with oxygen and form water vapour. Since there are no oxide ions transported to the anode, sulfur dioxide formation is suppressed [23–26]. In combination with the rather high operation temperature (typically 350 – 800 °C [27]), PCFCs are hence particularly interesting for the application of alternative fuels in which the presence of low H_2S concentrations cannot be avoided. The prospect of sulfur containing proton conducting electrolytes which may be stable under H_2S-rich conditions has recently been investigated by first-principle calculations [28].

Strontium ferrite partially substituted with molybdenum is known for its mixed electronic-ionic conductivity and stability over a wide range of oxygen partial pressures [29–33]. Reported conductivity values for $SrFe_{0.75}Mo_{0.25}O_{3-\delta}$ (SFM) lie in the order of 0.1 S/cm at 400-800 °C in both oxidising (air) and reducing (dry 5% H_2) conditions [31]. The electronic conductivity in strontium ferrites is dominated by a small polaron hopping [30,34]. Under

2

oxidizing conditions, the material is predominantly a p-type conductor where hole polarons jump between Fe^{3+} and Fe^{4+} ions, whereas electrons jump between Fe^{2+} and Fe^{3+} in the n-type regime at low oxygen partial pressures. In both cases, the ionic conductivity is about two orders of magnitude lower than the electronic [30]. These properties make SFM an interesting candidate for electrode materials in SOFCs [31,33,35]. Zheng et al. [33,35] recently investigated an SOFC with symmetric SFM electrodes and a $Ce_{0.8}Gd_{0.2}O_{1.9}$ electrolyte and obtained a peak power density of about 15 mW/cm^2 at 800 °C. The effects of various biogas components, including CO, CH_4 [33,35] and H_2S [35], were studied and Mo-doped strontium ferrites were found to be coke resistant. SFM electrodes were exposed to 800 ppm H_2S for 12 h under steam reforming conditions and characterized by thermogravimetry (TG) and X-ray photoelectron spectroscopy (XPS): sulfur-containing compounds were formed on the surface, but the overall microstructure of the material remained quite intact. Considering the high concentration of H_2S in those experiments (800 ppm), SFM may be a promising H_2S tolerant electrode material.

The influence of H_2S on the performance of the SFM anode in a fuel cell has, however, not yet been investigated. Here, we present studies of symmetric PCFCs with SFM electrodes and $BaZr_{0.8}Ce_{0.1}Y_{0.1}O_{3-\delta}$ electrolyte. The stability and performance of the button cell were investigated in the presence of 500 and 5000 ppm H_2S in the fuel.

2. Experimental

2.1. $SrFe_{0.75}Mo_{0.25}O_{3-\delta}$ materials synthesis

$SrFe_{0.75}Mo_{0.25}O_{3-\delta}$ (SFM) powders were synthesized according to a solid state reaction method. First, stoichiometric amounts of $SrCO_3$ (Aldrich, 99.9%), Fe_2O_3 (Alfa Aesar, 99.5%) and MoO_3 (Alfa Aesar, 99.5%) were weighed and milled in isopropanol for 2 h at 300 rpm in a planetary ball mill using agate balls and container. The obtained slurry was dried at 100 °C overnight in a heating cabinet. The resulting powders were ground in a mortar and uniaxially pressed into pellets and calcined in air at 1100 °C for 30 h. The pellets obtained from the calcination were crushed, milled and dried in a process analogous to that before the calcination. The phase purity of the synthesized powder was characterized by X-ray diffraction (XRD) using a Bruker D8 Discover with a Cu Kα radiation source in a 2Θ range of 10–90° and a scan step of 0.05°.

2.2. Cell fabrication

The electrolytes used in this study were $BaZr_{0.8}Ce_{0.1}Y_{0.1}O_{3-\delta}$ (BZCY81) pellets fabricated by CoorsTek (USA) according to a solid state reactive sintering method with NiO as a sintering aid. The sintering was followed by NiO leaching process resulting in a virtually Ni-free electrolyte with a relative density higher than 95% [36]. The thickness of the pellets was about 1.2 mm.

The chemical compatibility between SFM and $BaZr_{0.85}Y_{0.15}O_{3-\delta}$ (BZY) was investigated by firing 1:1 wt.% powder mixtures at different temperatures. BZY powder from CerPoTech (Norway) and SFM powder were mixed and milled in isopropanol at 350 rpm for 30 minutes using the same ball mill. The slurry obtained from milling was then dried overnight at 120 °C. The dried powders were fired at 1200 and 1400 °C for 2 hours and XRD measurements were performed after each firing.

For the electrodes, inks were prepared as a suspension of electrode powder in an organic ink vehicle, VEH (NexTech Materials). A BZY-SFM interlayer between the electrolyte and the electrodes was introduced in order to compensate for the thermal mismatch between the SFM and BZCY81, which otherwise would lead to delamination of the electrode in fuel cells if the SFM layer was deposited directly on the electrolyte. The thermal expansion coefficient (TEC) of SFM is reported to be 15.8×10^{-6} K^{-1} in the temperature range of 25–800 °C [35], whereas $BaZrO_3$-related compounds typically exhibit TEC values of 7–9 10^{-6} K^{-1} in the same temperature range [37–39]. Accordingly, two types of inks were made for application on the electrolyte pellet: the first layer from an ink consisting of 1:1 wt.% SFM and BZY, and the second layer of an ink with pure SFM.

An optimized fuel cell preparation procedure was realized via a two-step electrode deposition. In the first step, a layer of SFM–BZY ink was painted on each side of the electrolyte pellet and fired at 1200 °C for 5 h. In the second step, a layer of SFM ink was painted on the SFM-BZY layers and fired under the same conditions. This fabrication process thereby resulted in a symmetric SFM|SFM-BZY|BZCY81|SFM-BZY|SFM cell, with an electrode area of 0.5 cm^2. The estimated thicknesses of the SFM and SMF-BZY layers were 40 and 10 μm, respectively.

2.3. Materials and fuel cell performance characterization

The conductivity of the electrolyte was measured in order to determine the influence of H_2S on its electrical properties. A BZCY81 sample of 1.2 mm thickness was measured from 800 to 500 °C using a ProboStat sample holder (NorECs, Norway) in a standard two-electrode

4

four-wire setup with Au paint and mesh as electrodes ($\varnothing$ = 8 mm) using a HIOKI, IM 3533-01 LCR METER (10 kHz).

The gas compositions were controlled by a two-stage gas mixing system. First, a mixture of H_2 and Ar was passed through a saturated aqueous KBr solution, yielding gas mixtures with approx. 2.5% H_2O (80% relative humidity at room temperature). The wetted gas was subsequently mixed with a dry premixed gas of 1% H_2S in Ar in ratios yielding final H_2S contents of 500 and 5000 ppm. Due to this second mixing stage, the final concentration of H_2O was lowered to approx. 1.3 % in the 5000 ppm H_2S mixture, while it was essentially unchanged at approximately 2.5% in the 500 ppm H_2S mixture.

The microstructures of the SFM electrodes before and after fuel cell tests were studied by means of scanning electron microscopy (SEM) supported by energy dispersive X-ray spectroscopy (EDS) using a FEI Quanta FEG 200 microscope in high vacuum mode.

The fuel cells were studied by measuring the open circuit voltage (OCV), I-V curves, and the electrochemical impedance. All of these measurements were performed with different modules of a Gamry Reference 3000 Potentiostat. The I-V curves were measured by varying the voltage applied across the button cells (fuel cell mode) in the range from 0 to 0.9 V with a 2 mV step while the current was recorded. Impedance spectroscopy was performed under open-circuit conditions in the 0.01 Hz – 1 MHz range with 25 mV rms amplitude. The impedance data were deconvoluted using the Equivalent Circuit for Windows software [40]. Model circuits used for fitting were typically a series of inductance (L) and ohmic resistance (R_{Ohm}) elements followed by a series of (RQ) elements. An (RQ) element is a parallel connection of a resistor, R, and a capacitive constant phase element, Q. The total electrode polarisation resistance of the fuel cell, R_{pol}, containing contributions from both anode and cathode, was determined as the sum of all resistances from the (RQ) elements. The ohmic and polarization resistances were then normalized by the electrode surface area to obtain area specific resistances (ASR).

3. Results

Fig. 1 presents AC conductivity of the BZCY81 electrolyte as a function of temperature under wet reducing conditions and with 500 and 5000 ppm H_2S. Overall, it is clear that H_2S does not have a significant impact on the conductivity. In the most extreme case, when 5000 ppm H_2S was introduced into the gas mixture at 800 °C, the change in conductivity was not larger than 30% of the initial value. Moreover, this change cannot be attributed solely to the H_2S introduction but may reflect the simultaneous change in water vapour concentration from

5

2.5 % to 1.3 %, which can be expected to result in a drop in the total conductivity of a proton conductor due to dehydration, see e.g. [41]. Therefore, any effect of H_2S itself would be less pronounced than that observed in Fig. 1 and the differences in the measured conductivities with and without H_2S are not sufficiently consistent to be considered significant.
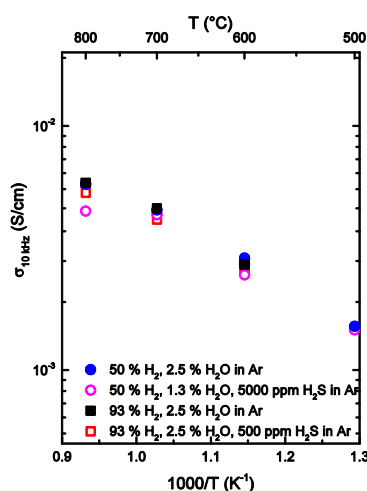

Figure 1. 10 kHz AC conductivity of BZCY81 electrolyte as a function of temperature in wet reducing conditions with 0, 500 and 5000 ppm H_2S.

Fig. 2 a presents the XRD pattern of as synthesized SFM powder, displaying the *Pm-3m* perovskite structure characteristic for this compound [35], and no impurities were detected. Fig. 2 b shows the result of XRD measurement of the mixture of SFM and BZY before and after firing at 1200 °C and 1400 °C for 2 hours. It can be seen that the mixture shows two clearly distinguishable patterns of SFM and BZY before firing. The diffractogram also shows peaks which can be attributed to $BaCO_3$. These probably originate from the carbonates formed on the surface of barium zirconate [42–44]. Nevertheless, the carbonate phase disappears after firing and does not affect the experiment outcome. The shift in the peak positions after firing at 1200 °C indicates interdiffusion between the two phases. However, two distinct phases are still observed, whereas at 1400 °C a new phase is formed. Therefore, 1200 °C is suggested as a maximum temperature for fabrication of fuel cells of BZY-based electrolytes and SFM electrodes. At temperatures lower than 1200 °C, sufficient adhesion of electrode layers to the electrolyte could not be obtained even for prolonged sintering times.
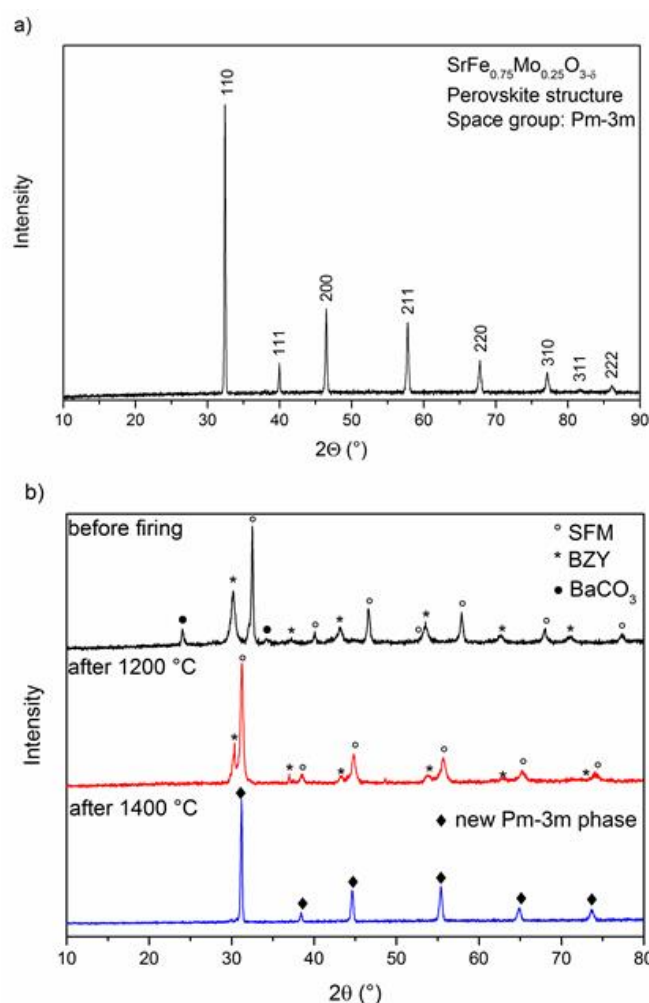
Figure 2. X-ray powder diffraction patterns: (a) $SrFe_{0.25}Mo_{0.25}O_{3-\delta}$ (SFM), (b) a BZY-SFM powder mixture before and after firing for 2 hours at 1200 °C and 1400 °C.

The fabricated cells consist of two SFM electrodes deposited symmetrically on each side of the BZCY81 electrolyte (Fig. 3 a). SEM micrographs of the cross-section of the fuel cell are presented in Fig. 3 b, which clearly shows the layers of SFM, SFM-BZY cercer and the electrolyte. The EDS line scan across the layers (denoted I, II and III in Fig. 3 c and d) confirms that there was no significant interdiffusion of the metal cations between the different layers during the fabrication process. A top view of the SFM and SFM-BZY layers is shown in Fig. 3 e. The SFM-BZY layer was usually slightly larger in diameter than the top SFM layer. Fig. 3 f shows the microstructure of an SFM layer before fuel cell operation which exhibits good connectivity between SFM grains and open porosity.
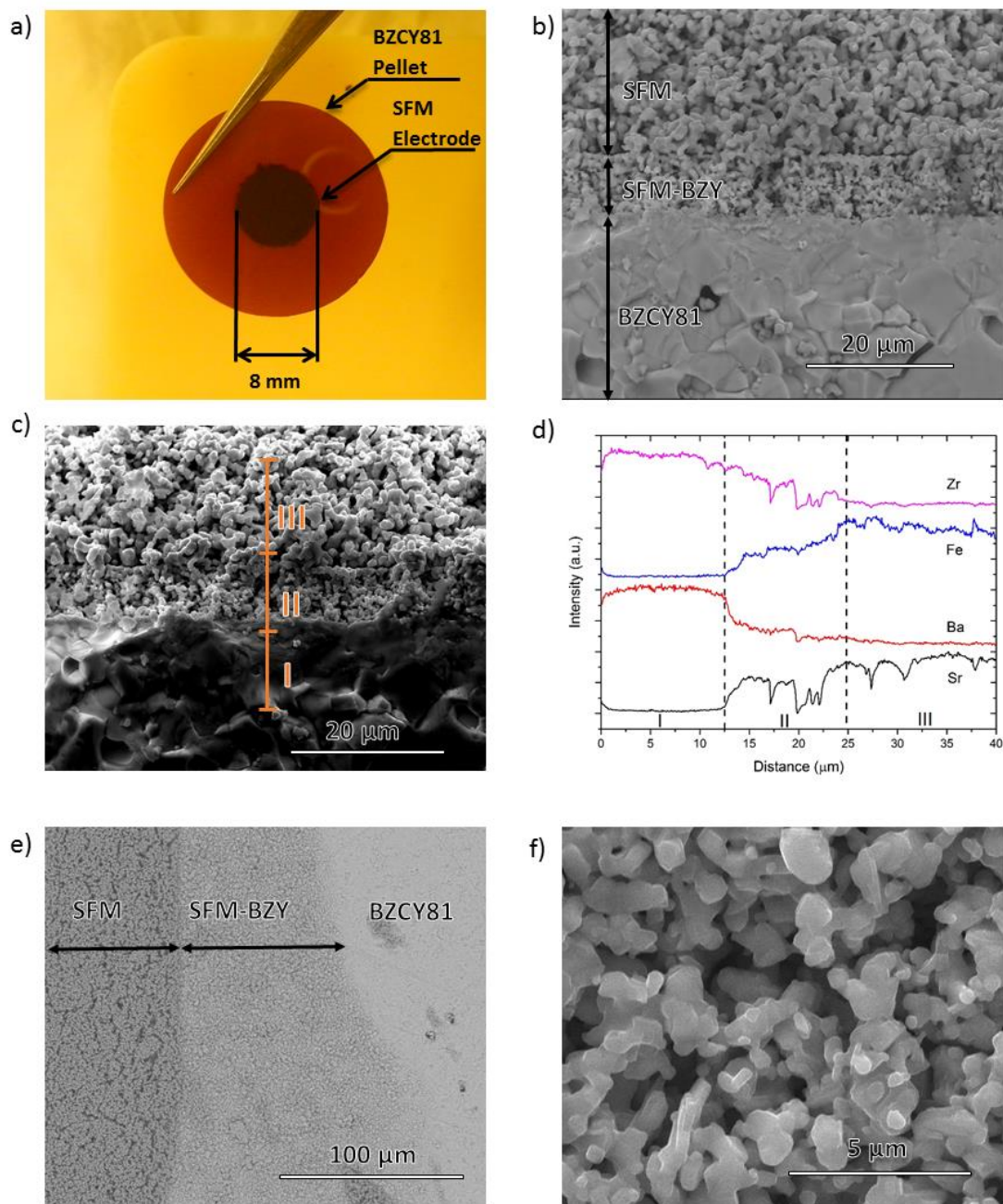
7

Figure 3. The fabricated fuel cell: top-view picture of the button cell (a), SEM micrograph of the cross-section (b), cross-section showing EDS line scan regions (c), EDS line scan of the cross-section (d), top-view of the deposited layers (e) and microstructure of the SFM layer (f).

8

Fig. 4 presents electrical properties of the fuel cells measured with wet 50 % H_2 in Ar used as the fuel and wet air as the oxidant. A typical measured impedance spectrum is presented in Fig. 4 a, and the applied model circuit represents the measured data quite well. ASR_{ohm} and ASR_{pol} are plotted as a function of inverse absolute temperature in Fig. 4 b. The slight reduction in OCV at a higher temperature may be ascribed to increasing electronic leak at higher temperature [45], or slight variations in the chemical activity of the gases due to gas leakages between the two chambers.
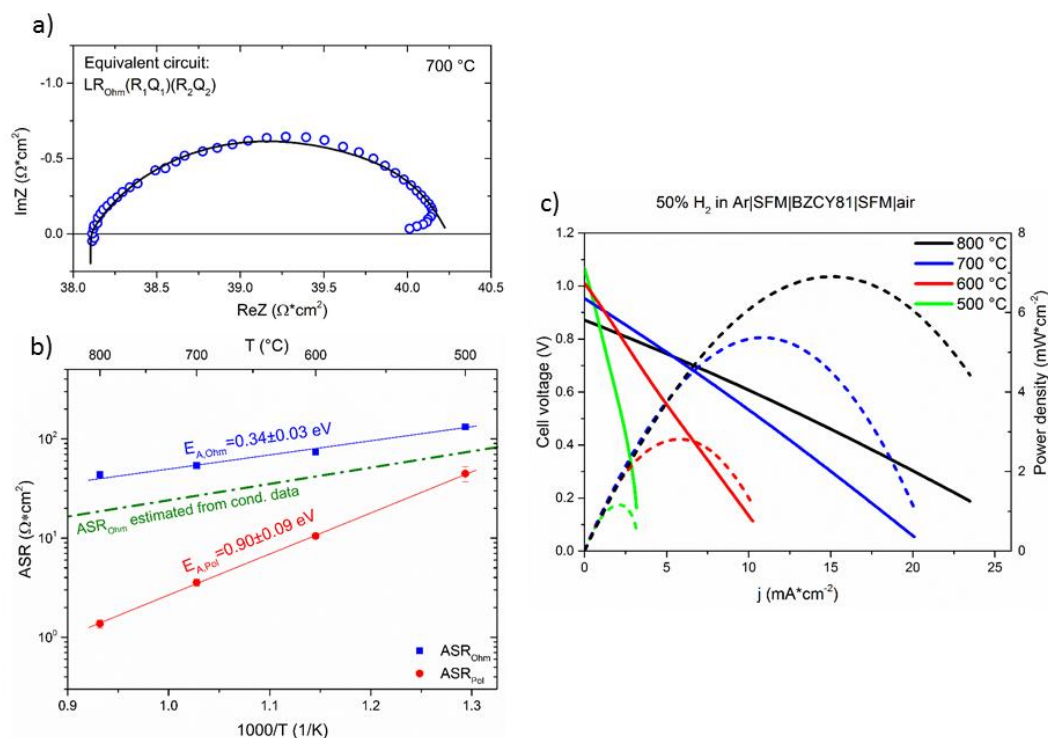

Figure 4. Electrical properties of the button cells under wet H_2 in Ar as fuel and wet air as oxidant: (a) impedance complex plot measured at 700 °C (○) with fitting curve (line), (b) ASR_{ohm} and ASR_{pol} plotted as a function of inverse absolute temperature and (c) typical I-V curve (line) and power output (dashed line) of the button cells.

The lower limit of ohmic resistance for the fuel cell where only the electrolyte contributes was estimated from the electrolyte conductivity data from Fig. 1 and is represented by the dashed line in Fig. 4 b. One can see that the measured and estimated ohmic resistances exhibit essentially the same activation energy and the difference between these values are within one order of magnitude. This means that the major contribution to the total resistance of the cell comes from the rather thick electrolyte, which in turn will limit the fuel cell performance in terms of power density.

9

A qualitative comparison of the obtained fuel cell characteristics can be made with the work of Zheng et al. [35] who investigated SFM electrodes in a symmetric SOFC with Gd-doped CeO_2 electrolyte. The present PCFC study shows a lower activation energy (0.90 eV compared to 1.11 eV) and hence lower ASR_{pol} in the temperature range of 500-800 °C.

Fig. 4 c. presents a typical I-V curve together with a power output of one of the measured fuel cells. The maximum power density of the symmetric fuel cell reaches 5.4 and 6.9 mW/cm^2 at 700 °C and 800 °C, respectively.

Two different fuel cells were exposed to wet H_2-Ar mixtures containing 5000 and 500 ppm H_2S. The measured OCV of the fuel cell operating with fuel containing 5000 ppm H_2S is shown as a function of time in Fig. 5 a. At 800 °C, the introduction of H_2S caused a decrease in the OCV which gradually slowed down. After removal of H_2S, the OCV returned to 90% of its initial value. After this measurement, the temperature was decreased to 700 °C and the procedure was repeated. At 700 °C, the OCV dropped immediately upon introducing H_2S and then continued to decay more slowly than at 800 °C. A similar experiment with continuous monitoring of the OCV was conducted on another sample in fuel containing 500 ppm H_2S at 700 °C (Fig. 5 b). As with the previous experiment, the OCV decreased immediately after the introduction of H_2S and continued to decay, although slower than in 5000 ppm H_2S. Furthermore, fluctuations in the OCV signal were persistent and more prominent in the case of fuel with 500 ppm H_2S.
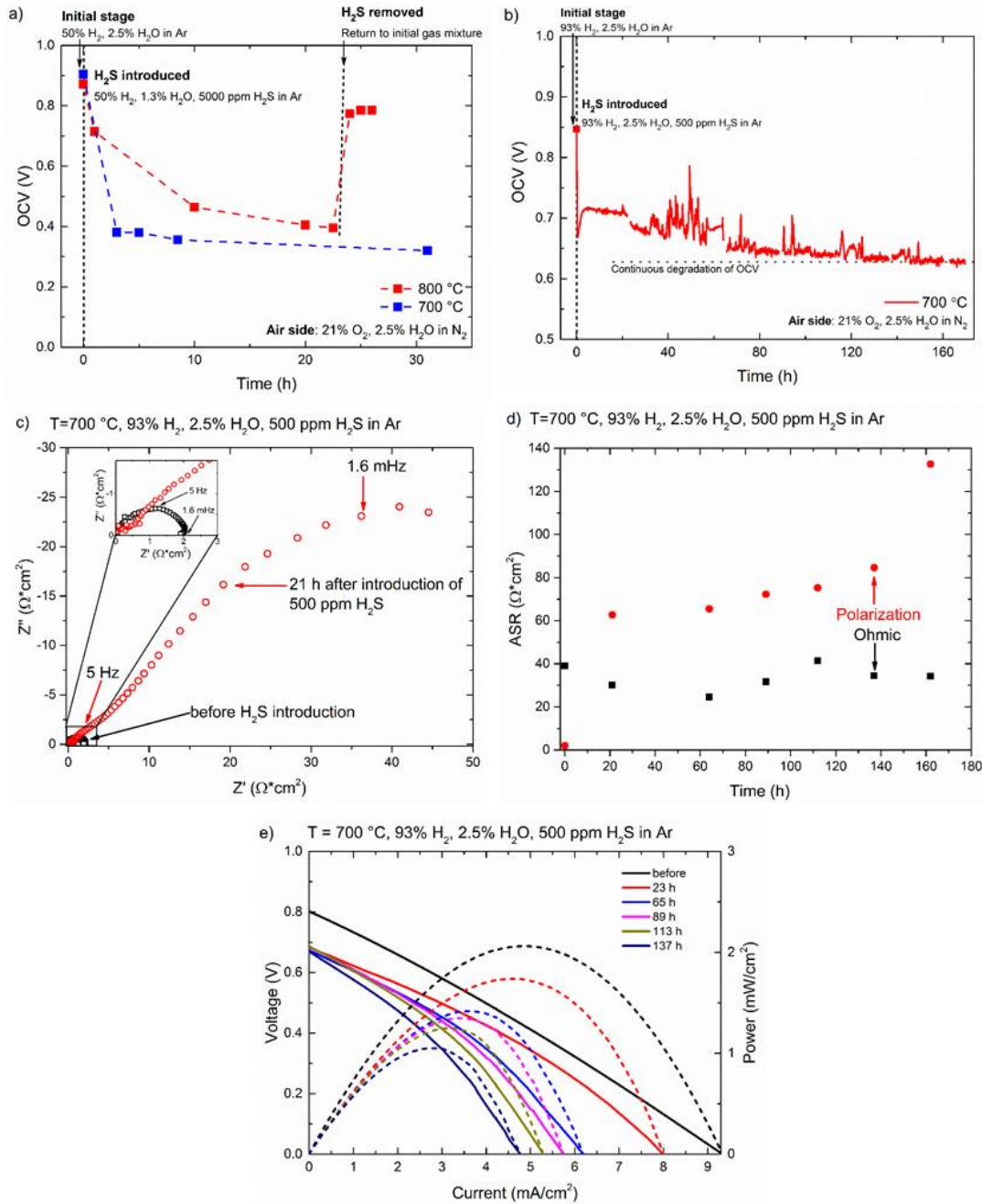
Figure 5. Influence of H₂S on performance of the fuel cells. Change in the OCV induced by presence of (a) 5000 and (b) 500 ppm H₂S in the fuel. Effect of the 500 ppm H₂S on (c) impedance complex plots, (d) ASR_ohm and ASR_pol and (e) I-V (solid) and power curves (dashed lines).

Electrochemical impedance spectroscopy showed that both the ohmic and polarization resistances were affected by H₂S. Fig. 5 c shows the impact of exposing the fuel cell to 500 ppm H₂S on an impedance complex plot before and after H₂S exposure. The ohmic part of the resistance was subtracted from the data in order to emphasise the change in ASR_pol. After H₂S

11

was introduced a new semicircle appeared in the low frequency range which caused the increase in ASR_{pol} as shown in Fig. 5 d. ASR_{ohm} (also presented in Fig. 5 d) fluctuated around a constant value and therefore seems comparatively less affected by H_2S.

The impact of H_2S on the power output of the fuel cell was also investigated. Fig. 5 e shows the influence of time of exposure to 500 H_2S on the I-V and power curves. The maximum current density and power output decrease with time of exposure. After 137 h of continuous operation in 500 ppm H_2S, the maximum power density had dropped to approximately half of its original value.

SEM images of the fuel cell anodes after operation in 500 and 5000 ppm H_2S are shown in Figs. 6 and 7, respectively. It is clear that exposure to H_2S has a severe impact on the microstructure of the anode. The electrodes did not exhibit the previously observed uniform microstructure of a porous backbone, and new regions with varying porosity appeared. Signs of delamination and cracking of the anode are also evident in the micrographs. Moreover, particles of a varying shape and size formed during operation are visible, e.g., tetragonal crystal grains (Fig. 6 c), whiskers (Fig. 6 c) and microplates (Fig 7 c).
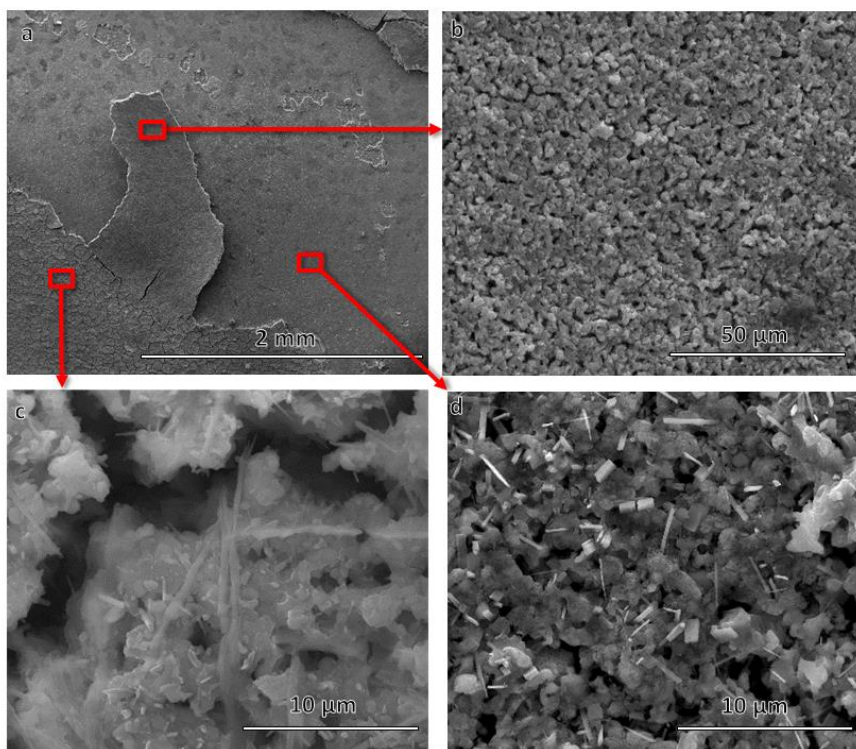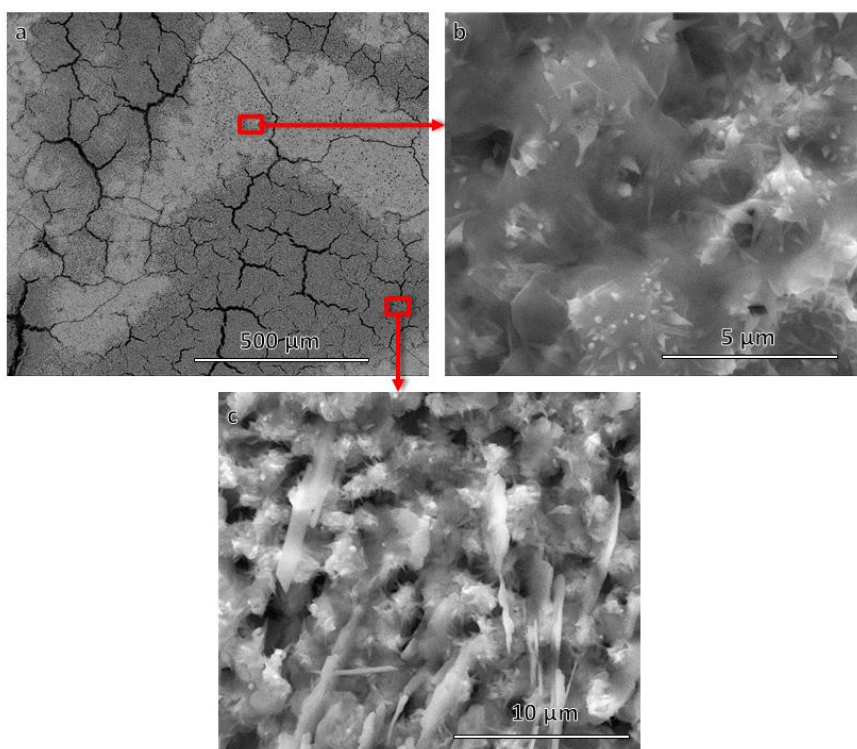

Figure 6. SEM images of the SFM anode after operation in the fuel containing 500 ppm H_2S with three highlighted regions at higher magnification (b-d).

Figure 7. SEM images of the SFM anode after operation in the fuel containing 5000 ppm H₂S with two highlighted regions at higher magnification (b,c).

The compositions of the regions shown in Figs. 6 b–d and 7 b–c were estimated by EDS as shown in Table 1. It is clear that the compositions differ among the regions. This was especially apparent for the fuel cell exposed to 5000 ppm H_2S (Fig. 7 a), in which the bright regions were enriched in Sr, whereas the dark regions contained more Fe. While EDS analysis is not reliable for quantification of oxygen content, qualitative comparisons can be made in the case of large differences. In general, the oxygen content in the electrode decreased with increasing H_2S concentration in the fuel. In the sample exposed to 500 ppm H_2S, the estimated oxygen content in the different regions varied between 7 and 29 %, whilst it was close to zero in the sample operating with 5000 ppm H_2S. This is consistent with a larger degree of sulfide formation in the presence of a higher H_2S content and a lower H_2O content. The particles visible in the micrographs usually had the same composition as the surrounding microstructure, which indicates that they are frontiers of growth of the new phase. The tetragonal grains (Fig. 6 c) differ in this respect, since they contain a much higher concentration of iron and sulfur than the surrounding area as shown by EDS.

Table 1. Results of EDS analyses of the regions presented in Figs. 6 and 7.

Elements	at. %				
	Fig. 6 b	**Fig. 6 c**	**Fig. 6 d**	**Fig. 7 b**	**Fig. 7 c**
Sr	46	35	43	48	16
Fe	20	9	3	1	21
Mo	9	9	6	n/a	n/a
Ba	1	6	3	5	46
Zr	3	16	4	26	<1
O	12	16	12	2	1
S	21	7	29	18	16

Post-operation XRD shows that new phases such as strontium, iron and molybdenum sulfides were formed (cf. Fig. 8). Both samples contain multiple phases and some of the XRD peaks could not be identified. The results could therefore only be analysed in a qualitative manner. The intensities of the peaks corresponding to the sulfide phases are generally higher for the sample exposed to higher H_2S concentration, i.e., 5000 ppm, and the intensity of the peaks attributed to SFM were correspondingly lower, in accordance with the SEM-EDS data. The peaks corresponding to barium zirconate (BZCY81 electrolyte and/or the BZY15 component of the electrode interlayer) are clearly visible in both cases and no sulfur-related compounds containing barium, zirconium or yttrium were detected.
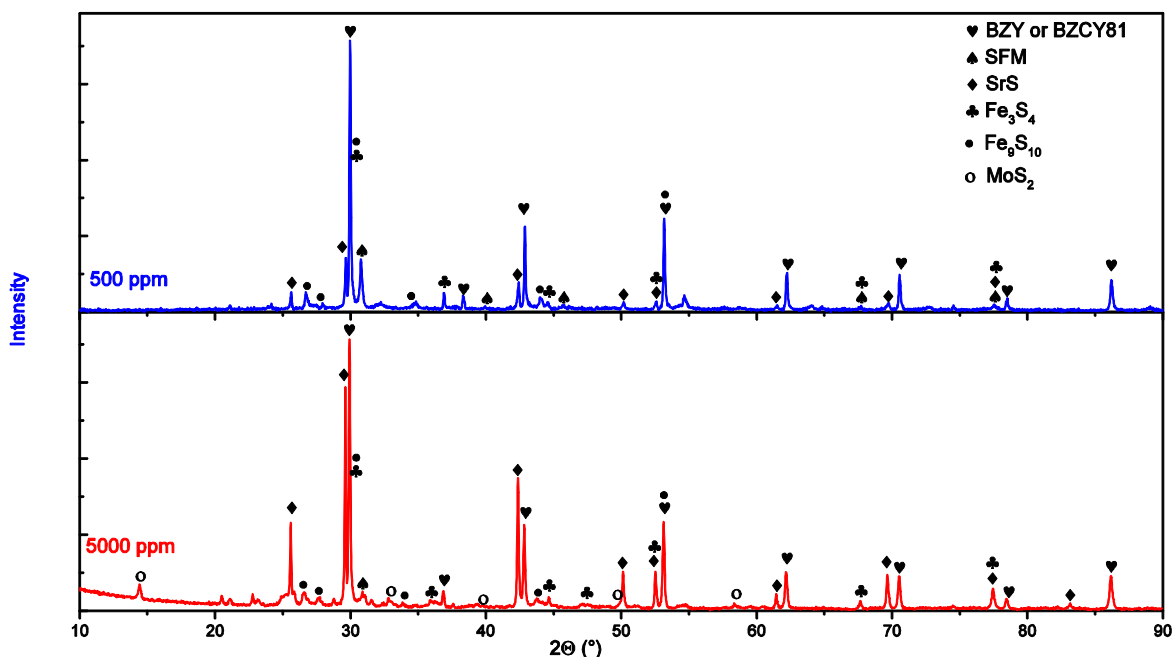
Figure 8. XRD patterns of the anode decomposition after exposure to fuel containing 500 and 5000 ppm H₂S.

4. Discussion

The measured OCV and power density showed continuous degradation of the fuel cells under H_2S exposure (cf. Fig. 5). Post-characterization of the anode by SEM showed that SFM degraded into metal sulfides during operation with H_2S. Considering the fact that the electrolyte conductivity was not significantly affected by H_2S, the reduced fuel cell performance can reasonably be attributed to the degradation of the SFM anode in the presence of H_2S.

The electrochemical impedance measurements showed an increase in the total polarization resistance in H_2S as demonstrated by a semicircle which appeared in the low frequency range. Low frequency semicircles are typically attributed to mass transport processes and correlated with the microstructure of the electrodes [46]. As shown in Figs. 6 and 7 the microstructure changed due to formation of sulfides. Therefore, the increased ASR_{pol} observed in Fig. 5 d may be explained by a continuous reaction of SFM to form sulfides and simultaneous degradation of the electrode microstructure, which may limit gas diffusion accordingly.

Another phenomenon observed during the operation – fluctuation in ASR_{ohm} – can also be explained by the formation of sulfides. The delamination of the electrode (Fig. 6 a) can be expected to lead to increased contact resistance due to a decrease in the effective anode area

15

and the apparent ASR_{ohm} will consequently increase. On the other hand, phase growth along the electrolyte surface would have the opposite effect, thereby causing the ASR_{ohm} fluctuations observed in Fig. 5 d. The magnitude of the measured OCV throughout the experiments can be affected by the presence of H_2S in several ways. According to the Nernst equation, the OCV relates to the net reaction over the cell and the activity of the gases for an electrolyte with a given charge carrier and transport number (here, notably protons). The experimental results indicate that upon introduction of H_2S, the electrode degradation reaction and changes in microstructure may affect the local chemical activity of gases due to gas diffusion limitations.

Another important aspect of the present study is the chemical stability of $BaZr_{0.8}Ce_{0.1}Y_{0.1}O_{3-\delta}$ (BZCY81) in H_2S atmospheres. There was no evidence of the BZCY81 electrolyte deterioration, even during prolonged experiments in sulfur-rich environments. Moreover, the conductivity did not change with hydrogen sulfide partial pressure. Perhaps the most interesting property of the studied system is that the fuel cell was still functioning even though the electrode material and microstructure degraded quite significantly. It seems that the formed sulfides were conductive and thereby served as functional anode materials. In particular, molybdenum and iron sulfides have previously been studied as candidates for fuel cell operating in H_2S-rich environment [11,47]. Therefore, fuel cells with electrodes comprising sulfides or mixed sulfide-oxide systems can be considered as a promising direction for developing H_2S-tolerant electrodes. This study may seem contradictory to the reported stability of SFM in up to 800 ppm H_2S by Zheng et al. [35]. This however can be explained by the difference in water vapour partial pressures since it is the H_2S/H_2O ratio in the gas phase that defines the relative activities of sulfur and oxygen for a given H_2 partial pressure. Zheng et al. used simulated steam reforming conditions with up to 22% steam, while the present work was focused on conditions typical for a PCFC where the water vapour content was lower than 3%. As a result, it may be concluded that SFM is not stable in H_2S-rich fuels as long as high levels of steam are not present. In comparison with other oxides studied in the literature, SFM has lower stability towards H_2S than doped lanthanum chromites [47,48], gadolinates [48] and vanadates [47,49] or La-doped strontium titanates [47]. Since many sulfur-tolerant perovskites contain La on the A-site, it may be a good strategy to dope SFM with this element in order to improve its tolerance towards sulfur.

The maximum power output of 5.4 mW/cm^2 at 700 °C is much lower than the best PCFCs operated without H_2S [27,50,51]. This can be explained by the high ohmic resistance caused by our rather thick electrolyte. By using an electrode-supported fuel cell with a 10-µm-thick

electrolyte, the estimated maximum power density would be around 100 mW/cm^2 with the electrodes applied here. It should also be noted that the fuel cells in this study were not optimized for power output. Given all of these aspects, the symmetric PCFC with SFM electrodes can be considered eligible for further studies.

5. Conclusions

Symmetric fuel cells with BZCY81 electrolyte and SFM electrodes were studied and the performance was measured with wet 50% H$_2$ in Ar as a fuel and wet air as an oxidant. The maximum power output of the fabricated fuel cell, 5.4 and 6.9 mW/cm^2 at 700 °C and 800 °C, respectively, was limited by the 1.2 mm thick electrolyte. The presence of H$_2$S in the fuel did not significantly affect the conductivity of BZCY81.

Introduction of H$_2$S into the fuel caused degradation of the SFM anode material. The fuel cell exposed to 500 ppm H$_2$S for 137 h degraded by 50% in terms of the maximum power output. Moreover, when 500 and 5000 ppm H$_2$S were introduced, the OCV of the fuel cell decreased from about 0.9 V to 0.6 and 0.4 V, respectively. Post-characterization of the anode showed that SFM had reacted with H$_2$S to form metal sulfides. Since the fuel cell was still functional after degradation, sulfides or mixed sulfide-oxide systems may be considered promising for novel H$_2$S-tolerant electrodes.

References

[1]   K.D. Kreuer, Fuel Cells: Selected Entries from the Encyclopedia of Sustainability Science and Technology, 2012. doi:10.1016/B978-044452745-5.00290-2.

[2]   M. Ball, M. Wietschel, The future of hydrogen – opportunities and challenges☆, Int. J. Hydrogen Energy. 34 (2009) 615–627. doi:10.1016/j.ijhydene.2008.11.014.

[3]   J. Molenda, J. Kupecki, R. Baron, M. Blesznowski, G. Brus, T. Brylewski, M. Bucko,

J. Chmielowiec, K. Cwieka, M. Gazda, A. Gil, P. Jasinski, Z. Jaworski, J. Karczewski, M. Kawalec, R. Kluczowski, M. Krauz, F. Krok, B. Lukasik, M. Malys, A. Mazur, A. Mielewczyk-Gryn, J. Milewski, S. Molin, G. Mordarski, M. Mosialek, K. Motylinski, E.N. Naumovich, P. Nowak, G. Pasciak, P. Pianko-Oprych, D. Pomykalska, M. Rekas, A. Sciazko, K. Swierczek, J. Szmyd, S. Wachowski, T. Wejrzanowski, W. Wrobel, K. Zagorski, W. Zajac, A. Zurawska, Status report on high temperature fuel cells in Poland – Recent advances and achievements, Int. J. Hydrogen Energy. (2017). doi:10.1016/j.ijhydene.2016.12.087.

[4]   Y. Shiratori, T. Ijichi, T. Oshima, K. Sasaki, Internal reforming SOFC running on biogas, Int. J. Hydrogen Energy. 35 (2010) 7905–7912. doi:10.1016/j.ijhydene.2010.05.064.

[5]   S. Rasi, A. Veijanen, J. Rintala, Trace compounds of biogas from different biogas production plants, Energy. 32 (2007) 1375–1380. doi:10.1016/j.energy.2006.10.018.

[6]   N. Abatzoglou, S. Boivin, A review of biogas purification processes, Biofuels, Bioprod. Biorefining. 3 (2009) 42–71. doi:10.1002/bbb.117.

[7]   A.M. Montebello, M. Fernández, F. Almenglo, M. Ramírez, D. Cantero, M. Baeza, D. Gabriel, Simultaneous methylmercaptan and hydrogen sulfide removal in the desulfurization of biogas in aerobic and anoxic biotrickling filters, Chem. Eng. J. 200–202 (2012) 237–246. doi:10.1016/j.cej.2012.06.043.

[8]   R.A. Pandey, S. Malhotra, Desulfurization of Gaseous Fuels with Recovery of Elemental Sulfur: An Overview, Crit. Rev. Environ. Sci. Technol. 29 (1999) 229–268. doi:10.1080/10643389991259236.

[9]   WHO World Health Organization, WHO Regional Publications, European Series; No. 91: Air quality guidelines for Europe, 2000. doi:10.1007/BF02986808.

[10]   M. Arnold, Reduction and monitoring of biogas trace compounds, Espoo, 2009. http://www.vtt.fi/inf/pdf/tiedotteet/2009/T2496.pdf.

[11]   J.P. Trembly, A.I. Marquez, T.R. Ohrn, D.J. Bayless, Effects of coal syngas and H2S on the performance of solid oxide fuel cells: Single-cell tests, J. Power Sources. 158 (2006) 263–273. doi:10.1016/j.jpowsour.2005.09.055.

[12]   S. Zha, Z. Cheng, M. Liu, Sulfur Poisoning and Regeneration of Ni-Based Anodes in Solid Oxide Fuel Cells, J. Electrochem. Soc. 154 (2007) B201. doi:10.1149/1.2404779.

[13]   Y. Matsuzaki, The poisoning effect of sulfur-containing impurity gas on a SOFC
anode: Part I. Dependence on temperature, time, and impurity concentration, Solid
State Ionics. 132 (2000) 261–269. doi:10.1016/S0167-2738(00)00653-6.

[14]   Z. Cheng, M. Liu, Characterization of sulfur poisoning of Ni–YSZ anodes for solid
oxide fuel cells using in situ Raman microspectroscopy, Solid State Ionics. 178 (2007)
925–935. doi:10.1016/j.ssi.2007.04.004.

[15]   S. Hernández, L. Solarino, G. Orsello, N. Russo, D. Fino, G. Saracco, V. Specchia,
Desulfurization processes for fuel cells systems, Int. J. Hydrogen Energy. 33 (2008)
3209–3214. doi:10.1016/j.ijhydene.2008.01.047.

[16]   D. Mescia, S.P. Hernández, A. Conoci, N. Russo, MSW landfill biogas desulfurization,
Int. J. Hydrogen Energy. 36 (2011) 7884–7890. doi:10.1016/j.ijhydene.2011.01.057.

[17]   L. Barelli, G. Bidini, F. Gallorini, S. Servili, Hydrogen production through sorption-
enhanced steam methane reforming and membrane technology: A review, Energy. 33
(2008) 554–570. doi:10.1016/j.energy.2007.10.018.

[18]   M. Komiyama, T. Misonou, S. Takeuchi, K. Umetsu, J. Takahashi, Biogas as a
reproducible energy source: Its steam reforming for electricity generation and for farm
machine fuel, Int. Congr. Ser. 1293 (2006) 234–237. doi:10.1016/j.ics.2006.03.008.

[19]   J. Van herle, F. Maréchal, S. Leuenberger, Y. Membrez, O. Bucheli, D. Favrat, Process
flow model of solid oxide fuel cell system supplied with sewage biogas, J. Power
Sources. 131 (2004) 127–141. doi:10.1016/j.jpowsour.2004.01.013.

[20]   S. Wang, G.Q. Lu, G.J. Millar, Carbon Dioxide Reforming of Methane To Produce
Synthesis Gas over Metal-Supported Catalysts: State of the Art, Energy & Fuels. 10
(1996) 896–904. doi:10.1021/ef950227t.

[21]   J. Xuan, M.K.H. Leung, D.Y.C. Leung, M. Ni, A review of biomass-derived fuel
processors for fuel cell systems, Renew. Sustain. Energy Rev. 13 (2009) 1301–1313.
doi:10.1016/j.rser.2008.09.027.

[22]   J. Van herle, Y. Membrez, O. Bucheli, Biogas as a fuel source for SOFC co-generators,
J. Power Sources. 127 (2004) 300–312. doi:10.1016/j.jpowsour.2003.09.027.

[23]   W.F. Giauque, E.W. Hornung, J.E. Kunzler, T.R. Rubin, The Thermodynamic
Properties of Aqueous Sulfuric Acid Solutions and Hydrates from 15 to 300°K., J. Am.

Chem. Soc. 82 (1960) 62–70. doi:10.1021/ja01486a014.

[24] T.R. Rubin, W.F. Giauque, The Heat Capacities and Entropies of Sulfuric Acid and Its Mono- and Dihydrates from 15 to 300°K., J. Am. Chem. Soc. 74 (1952) 800–804. doi:10.1021/ja01123a063.

[25] G.E. Walrafen, D.M. Dodd, Infra-red absorption spectra of concentrated aqueous solutions of sulphuric acid. Part 2.—H 2 SO 4 and HSO–4 vibrational fundamentals and estimates of (F°298·15—H°0)/T and S°298·15 for H 2 SO 4 gas, Trans. Faraday Soc. 57 (1961) 1286–1296. doi:10.1039/TF9615701286.

[26] J.R. Eckman, F.D. Rossini, The heat of formation of sulphur dioxide, Bur. Stand. J. Res. 3 (1929) 597–618.

[27] C. Duan, J. Tong, M. Shang, S. Nikodemski, M. Sanders, S. Ricote, A. Almansoori, R. OHayre, Readily processed protonic ceramic fuel cells with high performance at low temperatures, Science (80-.). 349 (2015) 1321–1326. doi:10.1126/science.aab3987.

[28] J.M. Polfus, T. Norby, R. Bredesen, Protons in Oxysulfides, Oxysulfates, and Sulfides: A First-Principles Study of La 2 O 2 S, La 2 O 2 SO 4 , SrZrS 3 , and BaZrS 3, J. Phys. Chem. C. 119 (2015) 23875–23882. doi:10.1021/acs.jpcc.5b08278.

[29] A.A. Markov, O.A. Savinskaya, M.V. Patrakeev, A.P. Nemudry, I.A. Leonidov, Y.T. Pavlyukhin, A.V. Ishchenko, V.L. Kozhevnikov, Structural features, nonstoichiometry and high-temperature transport in SrFe1−xMoxO3−δ, J. Solid State Chem. 182 (2009) 799–806. doi:10.1016/j.jssc.2008.12.026.

[30] A.A. Markov, I.A. Leonidov, M.V. Patrakeev, V.L. Kozhevnikov, O.A. Savinskaya, U.V. Ancharova, A.P. Nemudry, Structural stability and electrical transport in SrFe1−xMoxO3−δ, Solid State Ionics. 179 (2008) 1050–1053. doi:10.1016/j.ssi.2008.01.026.

[31] A.J. Fernández-Ropero, J.M. Porras-Vázquez, A. Cabeza, P.R. Slater, D. Marrero-López, E.R. Losilla, High valence transition metal doped strontium ferrites for electrode materials in symmetrical SOFCs, J. Power Sources. 249 (2014) 405–413. doi:10.1016/j.jpowsour.2013.10.118.

[32] O.V. Merkulov, E.N. Naumovich, M.V. Patrakeev, A.A. Markov, H.J.M. Bouwmeester, I.A. Leonidov, V.L. Kozhevnikov, Oxygen nonstoichiometry and defect chemistry of perovskite-structured SrFe1−xMoxO3−δ solid solutions, Solid State

Ionics. 292 (2016) 116–121. doi:10.1016/j.ssi.2016.05.009.

[33] K. Zheng, K. Świerczek, N.M. Carcases, T. Norby, Coking Study in Anode Materials for SOFCs: Physicochemical Properties and Behavior of Mo-Containing Perovskites in CO and CH4 Fuels, ECS Trans. 64 (2014) 103–116. doi:10.1149/06402.0103ecst.

[34] M. Patrakeev, I. Leonidov, V. Kozhevnikov, V. Kharton, Ion–electron transport in strontium ferrites: relationships with structural features and stability, Solid State Sci. 6 (2004) 907–913. doi:10.1016/j.solidstatesciences.2004.05.002.

[35] K. Zheng, K. Świerczek, J.M. Polfus, M.F. Sunding, M. Pishahang, T. Norby, Carbon Deposition and Sulfur Poisoning in SrFe0.75Mo0.25O3- and SrFe0.5Mn0.25Mo0.25O3- Electrode Materials for Symmetrical SOFCs, J. Electrochem. Soc. 162 (2015) F1078–F1087. doi:10.1149/2.0981509jes.

[36] Coorstek Inc., Manufacturer's datasheet: BZCY81 Ni-leeched pellet, 2015.

[37] J.M. Serra, W.A. Meulenberg, Thin-Film Proton BaZr 0.85 Y 0.15 O 3 Conducting Electrolytes: Toward an Intermediate-Temperature Solid Oxide Fuel Cell Alternative, J. Am. Ceram. Soc. 90 (2007) 2082–2089. doi:10.1111/j.1551-2916.2007.01677.x.

[38] Y. Zhao, D. Weidner, Thermal expansion of SrZrO3 and BaZrO3 perovskites, Phys. Chem. Miner. 18 (1991). doi:10.1007/BF00200187.

[39] S. Yamanaka, M. Fujikane, T. Hamaguchi, H. Muta, T. Oyama, T. Matsuda, S. Kobayashi, K. Kurosaki, Thermophysical properties of BaZrO3 and BaCeO3, J. Alloys Compd. 359 (2003) 109–113. doi:10.1016/S0925-8388(03)00214-7.

[40] B. Boukamp, A package for impedance/admittance data analysis, Solid State Ionics. 18–19 (1986) 136–140. doi:10.1016/0167-2738(86)90100-1.

[41] A. Magrasó, C. Kjølseth, R. Haugsrud, T. Norby, Influence of Pr substitution on defects, transport, and grain boundary properties of acceptor-doped BaZrO3, Int. J. Hydrogen Energy. 37 (2012) 7962–7969. doi:10.1016/j.ijhydene.2011.10.067.

[42] R. Sažinas, C. Bernuy-López, M.-A. Einarsrud, T. Grande, Effect of CO 2 Exposure on the Chemical Stability and Mechanical Properties of BaZrO 3 -Ceramics, J. Am. Ceram. Soc. 99 (2016) 3685–3695. doi:10.1111/jace.14395.

[43] A. Ubaldini, V. Buscaglia, C. Uliana, G. Costa, M. Ferretti, Kinetics and Mechanism of Formation of Barium Zirconate from Barium Carbonate and Zirconia Powders, J. Am.

Ceram. Soc. 86 (2003) 19–25. doi:10.1111/j.1151-2916.2003.tb03271.x.

[44] Y. Yamazaki, R. Hernandez-Sanchez, S.M. Haile, High Total Proton Conductivity in Large-Grained Yttrium-Doped Barium Zirconate, Chem. Mater. 21 (2009) 2755–2762. doi:10.1021/cm900208w.

[45] S. Ricote, N. Bonanos, H.J. Wang, R. Haugsrud, Conductivity, transport number measurements and hydration thermodynamics of $BaCe0.2Zr0.7Y(0.1 - \xi)Ni \xi O(3 - \delta)$, Solid State Ionics. 185 (2011) 11–17. doi:10.1016/j.ssi.2010.12.012.

[46] M. Marrony, P. Berger, F. Mauvy, J.-C. Grenier, N. Sata, A. Magrasó, R. Haugsrud, P.R. Slater, G. Taillades, J. Roziere, J. Dailly, N. Fukatsu, P. Briois, H. Matsumoto, M. Stoukides, Proton-Conducting Ceramics. From Fundamentals to Applied Research, Pan Stanford Publishing, Singapore, 2016.

[47] M. Gong, X. Liu, J. Trembly, C. Johnson, Sulfur-tolerant anode materials for solid oxide fuel cell application, J. Power Sources. 168 (2007) 289–298. doi:10.1016/j.jpowsour.2007.03.026.

[48] S. Wang, M. Liu, J. Winnick, Stabilities and electrical conductivities of electrode materials for use in H2S-containing gases, J. Solid State Electrochem. 5 (2001) 188–195. doi:10.1007/s100080000142.

[49] L. Aguilar, S. Zha, Z. Cheng, J. Winnick, M. Liu, A solid oxide fuel cell operating on hydrogen sulfide (H2S) and sulfur-containing fuels, J. Power Sources. 135 (2004) 17–24. doi:10.1016/j.jpowsour.2004.03.061.

[50] S.M. Babiniec, S. Ricote, N.P. Sullivan, Characterization of ionic transport through BaCe0.2 Zr0.7Y0.1O3−δ membranes in galvanic and electrolytic operation, Int. J. Hydrogen Energy. 40 (2015) 9278–9286. doi:10.1016/j.ijhydene.2015.05.162.

[51] W.G. Coors, Protonic ceramic fuel cells for high-efficiency operation with methane, J. Power Sources. 118 (2003) 150–156. doi:10.1016/S0378-7753(03)00072-7.